Electron−Atom Superelastic Scattering in Magnesium at Millielectron Volt Energies†

T. Baynard,‡ A. C. Reber,§ R. F. Niedziela,|| S. A. Darveau,⊥ B. Prutzman,# and R. S. Berry*,‡

Department of Chemistry and The James Franck Institute, The University of Chicago, Chicago, Illinois 60637, Department of Physics, Virginia Commonwealth University, Richmond, Virginia 23284, Department of Chemistry, DePaul University, Chicago, Illinois 60614, Department of Chemistry, The University of Nebraska at Kearney, Kearney, Nebraska 68849, and Department of Chemistry, Lehigh Carbon Community College, Schnecksville, Pennsylvania 18078

Received: July 17, 2007; In Final Form: September 16, 2007

The energy dependence of superelastic scattering is measured for electrons on Mg(3^1P) from threshold to 270 meV with a novel technique. The method uses photoelectrons produced by a narrow bandwidth laser as an approximately monoenergetic incident electron source to collide with excited atoms. Measurements are made at energies as low as 1.5 meV with a resolution of 1 meV near threshold. An efficient magnetic-bottle time-of-flight electron spectrometer allows for the simultaneous measurement of multiple scattering channels. Above-threshold ionization is also observed. The measured energy dependence for transitions from the 3^1P state to both the 3^3P and 3^1S are found to be inversely proportional to the energy from 10 to 270 meV. Below 10 meV, the dependencies are different, with the 3^3P transition having an $E^{-1/2}$ dependence and the 3^1S channel retaining an E^{-1} dependence.

1. Introduction

We have developed a novel experiment[1] that uses photoelectrons produced with a narrow bandwidth laser as an electron source[2] to study the threshold behavior of electron−atom superelastic scattering (SES). SES is a process in which internal energy in the target is converted to electron kinetic energy during the collision.[3−6] In the experiments discussed here, the excited atoms are produced by a laser tuned to the 3^1P state of Mg and the threshold electrons are produced either by the same laser or by another ionizing laser tuned to the desired energy. Nearly all of the scattered electrons are turned by an axially symmetric inhomogeneous magnetic field toward a microchannel plate detector which taken together form a magnetic bottle spectrometer (MBS).[7] While the incident electrons have threshold energies, the measured electrons of principal interest have been scattered to significantly higher energies, for which the MBS transmission is high and constant. The scattered electon energies are determined by their time-of-flight (TOF) in the MBS. This method yields electron−atom collision cross section measurements with high electron energy resolution.

Low-energy electron−atom collision studies have been largely limited to elastic collisions due to the experimental difficulties associated with producing low-energy, high-resolution electron beams. Previous work has focused on electron-impact excitation,[8−10] but resolution problems have prevented detailed threshold energy experiments. Leep and Gallagher previously investigated the inelastic energy dependence of magnesium from threshold to 1400 eV[10] with an energy resolution of 250 meV. Similar experiments were performed by Aleksakhin and co-workers[11,12] at an energy resolution of 200 meV. Recent work has been performed by Sullivan et al. using both crossed beams and electron transmission spectroscopy from threshold to 8 eV with a resolution of 30 meV.[9] Several other investigators have used tunable dye lasers to prepare excited atoms, thus opening new areas of investigation for electron−atom scattering experiments.[8,13,14] The energy dependence of cross sections found in these studies are consistent with theoretical **R** matrix results,[15] but the lack of electron resolution and noise in the optical excitation function have limited this work at extremely low energies. The use of photoelectron spectroscopy has been used previously in the study of electron−molecule attachment,[16] for cluster attachment,[17] and in the use of monochromatic sychrotron radiation in the near-threshold ionization of Ar.[18,19] The use of superelastic collisions with laser excited atoms has an extensive history, has been reviewed by Andersen et al.,[6] and has been used to study angular distributions from metastable states.[20,21]

A related method of studying the slow channel of threshold scattering is by photodetachment.[22−24] These studies allow for the accurate determination of both the behavior and range of the threshold energy dependence. Threshold photodetachment shows the importance of centrifugal barriers, although the number of channels one can study this way is limited. Rydberg scattering also allows for the study of the threshold energy dependence.[25,26] A highly excited Rydberg electron has sufficient separation from the atom that it, in some ways, effectively behaves as a free electron. These results showed that deviations from threshold law behavior may appear anywhere from about 0.1 meV to 50 eV.

The energy dependence of a cross section near threshold is of interest since it is primarily due to the density of states available for the specific escape mechanism of the process or of the incident mechanism in the SES case. Wigner demonstrated that the energy dependence of threshold processes does not require extensive knowledge about the reaction process.[27] The threshold laws arise specifically from the density of states near threshold, the states which the outgoing electron may

† Part of the "Giacinto Scoles Festschrift".
* Corresponding author.
‡ The University of Chicago.
§ Virginia Commonwealth University.
|| DePaul University.
⊥ The University of Nebraska at Kearney.
Lehigh Carbon Community College.

10.1021/jp075583e CCC: $37.00
Published on Web 11/07/2007

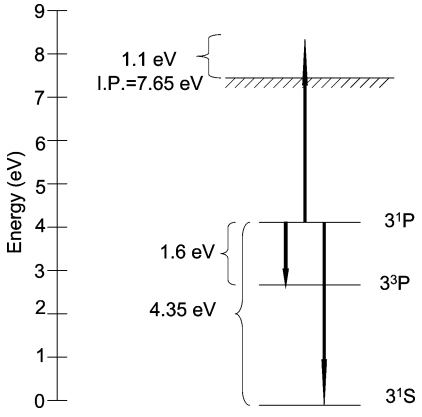

Figure 1. Sketch of the relevant energy levels and processes studied in the paper.

occupy, so long as the electron is outside of the influence of all shorter range potentials. By time reversal, for processes in which the projectiles collide at sufficiently low energies, the incoming potential is the source of the threshold law. The long-range escape potential of a process determines the energy dependence of the cross section from the threshold upward. How far upward is itself an interesting question, depending on the specific system. In the simplest case where the electron experiences only a short-range potential from the atom, the inelastic cross section, σ_{inel} has the form of eq 1

$$\sigma_{\text{inel}} \propto E^{l+1/2} \tag{1}$$

where E is the excess energy above threshold, and l is the angular momentum of the outgoing electron. The corresponding equation for the SES cross section, σ_{SES} is found through detailed balance to be as in eq 2, where l is the angular momentum of the incoming electron.[28]

$$\sigma_{\text{SES}} \propto E^{l-1/2} \tag{2}$$

In the polarization potential, the leading energy dependence of the cross section is the same as in eq 2; the primary effect of the second-order contributions to the potential is to restrict the range over which the threshold law is valid.[24] The dipole potential produces a threshold law which depends on the lowest eigenvalue of the dipole potential.[29,30] When the lowest eigenvalue of the wavefunction outside of the reaction sphere under the effect of a polarization potential is less than $-1/4$, then the threshold law is constant; if this eigenvalue is greater than $-1/4$, then the law is $\lambda_0 + 1$ where $\Lambda_0 = \lambda_0(\lambda_0 + 1)$,[30] where Λ_0 is the lowest eigenvalue. In the context of SES, the threshold law takes the dependence shown in eqs 3 and 4.

$$\sigma_{\text{SES}} \propto \frac{1}{E} \qquad \text{if } \Lambda_0 < \frac{1}{4} \tag{3}$$

$$\sigma_{\text{SES}} \propto E^{2\lambda_0 - 1/2} \qquad \text{if } \Lambda_0 > \frac{1}{4} \tag{4}$$

The threshold laws for SES are easily obtained via microscopic reversibility from the well-known threshold laws for inelastic scattering.[31]

In these experiments, three processes are observed. The first is two-photon, resonance-enhanced multiphoton ionization, REMPI. The second is REMPI followed by the SES of the photoelectron by a magnesium atom in the 3^1P state. The Mg energy levels are shown in Figure 1. The observed processes include both the de-excitation to the ground 3^1S state and to the 3^3P state, as shown in eqs 5 and 6, respectively.

$$\begin{aligned} \text{Mg}(3^1S) + h\nu_{\text{r}} &\rightarrow \text{Mg}^*(3^1P) \\ \text{Mg}^*(3^1P) + h\nu_{\text{nr}} &\rightarrow \text{Mg}^+ + \text{e}_{\text{C}}^- \\ \text{Mg}^*(3^1P) + \text{e}_{\text{t}}^- &\rightarrow \text{Mg}(3^1S) + \text{e}_{\text{A}}^- \end{aligned} \tag{5}$$

or

$$\text{Mg}^*(3^1P) + \text{e}_{\text{t}}^- \rightarrow \text{Mg}^{**}(3^3P) + \text{e}_{\text{B}}^- \tag{6}$$

where e_{A}^- and e_{B}^- are electrons released during de-excitation to the magnesium ground state and 3^3P states, respectively, and e_{t}^- corresponds to a threshold electron.

A third process observed in these experiments is above-threshold ionization (ATI).[32] ATI is a process in which an atom absorbs more than the minimum number of photons required for ionization. Absorption occurs when the electron being ejected is in the vicinity of its parent atom but is in a continuum state rather than a bound state. In this case, the excess energy is transferred into kinetic energy of the ejected electron. We observed two-photon ATI from the 3^1P state in magnesium,[33−35] as shown in eq 7.

$$\text{Mg}^*(3^1P) + 2h\nu_{\text{nr}} \rightarrow \text{Mg}^+ + \text{e}_{\text{r}}^- \tag{7}$$

where e_{r}^- is the electron released in the ATI process.

In this work, we present the energy dependence of SES cross sections from the 3^1P state to both the 3^3P and the 3^1S states from threshold to 270 meV. The threshold behavior of these channels was found, and the branching ratio of the two channels was measured as a function of energy. ATI was observed; although this process is not the primary focus of this project, it is included for mechanism comparison and analysis purposes. The cross sections were measured using resonant two-color two-photon ionization as the electron source. The electrons were detected by a magnetic bottle time-of-flight (TOF) spectrometer. This method allows for the incident electron resolution to be less than 6 meV for 1 eV electrons and approximately 1 meV for threshold electrons. This resolution allows for the threshold energy dependence of magnesium SES to be measured.

2. Experimental Section

The time-of-flight experiments were conducted with two photon sources, an effusive oven source, and a magnetic bottle spectrometer[7] as illustrated in Figure 2. Resonant radiation of wavelength 285.21 nm was generated by doubling the 570.42 nm output of a Continuum TDL51 tunable dye laser with a KDP crystal and used to prepare the 3^1P state in the target. This dye laser is pumped by the second harmonic of a Continuum YG661 Nd:YAG laser operating at 20 Hz with a pulse duration of about 8 ns. Ionizing photons were produced over a range between 335 and 376 nm by a Lumonics HD-300 tunable dye laser that is pumped by a Lumonics HE-420 XeCl excimer laser with a bandwidth of 0.02 meV. Laser dyes PTP, Exalite 351, DMQ, and Exalite 376 provide nearly complete coverage of the energy range up to 270 meV. The energies of the photoionization photons were measured using a McPherson monochromator with 0.1 nm resolution. The absolute uncertainty in the photoelectron energy was ±0.5 meV. The timing of the pulsed system was controlled using a Newport Model 818-BB20 fast photodiode with a 100 ps rise time and a Stanford DG535 dual delay module. The pulse durations for the resonant and ionization sources were 6.4 and 7.5 ns, respectively, with an uncertainty in relative timing of 1 ns. It should be noted that the lifetime of

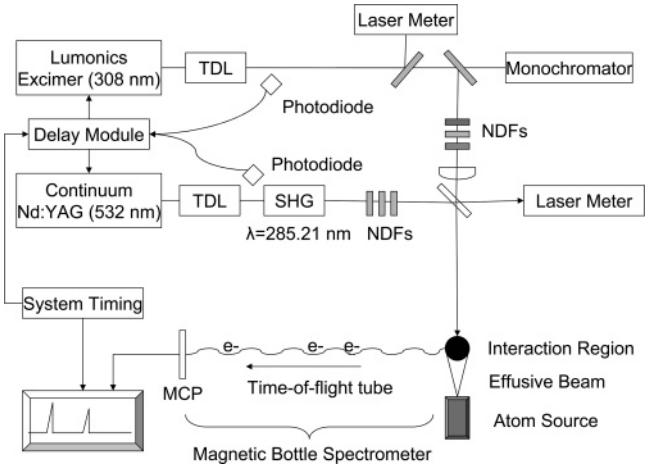

Figure 2. Schematic of the general experiment design. SHG is second harmonic generation; TDL is tunable dye laser; NDF is neutral density filter; and MCP is multichannel plate.

the 3^1P state of Mg is merely 2 ns. The laser power was measured using a Molectron J4−05 laser meter.

The two pulses are nearly collinear and aligned in time and space at the focus of the MBS. The ionization photon source is used to produce photoelectrons at the center of the interaction region which is defined by the overlap of the resonant photon beam, the region of the MBS mapped to the detector, and the atomic Mg vapor stream coming from a resistively heated oven operating between 650 and 850 K under effusive flow conditions.

Approximately 98% of the electrons ejected in the interaction region are collected by the MBS,[7] which is a 4 π steradian collecting version similar to that of Cheshnovsky's design.[37] In this case, however, we used a cobalt-samarium permanent magnet as the high-field source for the magnetic bottle.[38] The high field end of the MBS acts as a magnetic mirror reversing the velocity vectors of the electrons that are not initially moving toward the detector, a dual chevron multichannel plate (MCP). The magnetic field at the interaction region is 1200 G. An optional acceleration grid set at 0.4 V and located 1.2 cm upfield of the interaction region is used to improve real time measurement of the low-energy photoelectron signal. The electrons travel down a 57 cm flight tube surrounded by a solenoid that generates a magnetic field of 3 G. The acceleration grid did not effect the determined cross section of the SES, which was tested by comparing results from experiments with and without an applied potential. All other surfaces are grounded, and outside fields have negligible impact on the measurements. The efficiencies of the multichannel plate (55%) and two sets of wire mesh (86% each) that are used for electrically isolating the drift tube lead to an overall collection efficiency of approximately 36%.

Energy analysis is performed by measuring the time elapsed between the laser pulses and the arrival of the electrons. Signals from the MCP are sent to both a gated counter and a time-to-amplitude converter (TAC). The counter signal monitors the total electron count over a TOF period while the TAC measures the arrival time of the initial electron, thus allowing for the electron energy analysis. The determination of electron energies takes into account broadening of the TOF peak due to variations in the trajectories of the electrons, which is the main source for the observed peak structure in the TOF spectra. These variations are due to the angular distribution of the electrons, to the inhomogeneous magnetic field, and to the duration of the laser pulses.

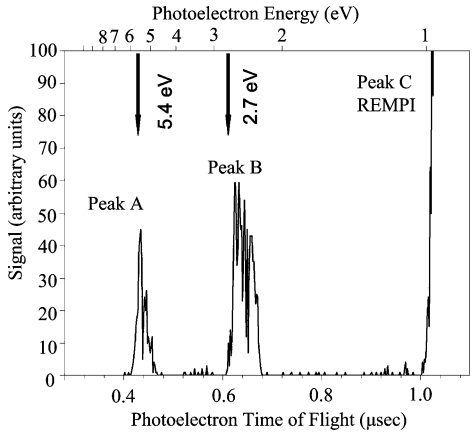

Figure 3. One-color time-of-flight spectrum with 1700 W/cm ^{2} 285.21 nm light and 2012 incident electrons per second.

The density of the atomic Mg vapor was determined using the photoionization signal from the prepared 3^1P state, the absolute cross section of which is $8.1 \pm (2.3 \times 10^{-17})$ cm^2 at 285.2 nm.[36] Due to saturation of the TAC, the absolute density could not be determined with sufficient accuracy to allow us to establish a reliable value of the absolute cross section. Nonetheless, the saturated TAC was able to determine relative changes in the density of the 3^1P state. Furthermore, while the TAC is saturated, the TOF spectrum was determined under conditions where roughly 5% of the pulses produced SES counts, so the statistics for the fast counts are unaffected. The atomic density is typically set to provide approximately 10^{10} atoms/cm^3, yielding 8% of the atoms in the excited state. Varying the temperature of the oven permitted a density dependence to be measured over an eightfold range.

The total cross section is determined by eq 8

$$\ln\left(\frac{R_0 - R_s}{R_0}\right) = -\sigma_{SES}\bar{\lambda}\rho_{Mg^*} \tag{8}$$

where R_0 is the rate of incident electrons, R_s is the rate of scattered electrons, $\bar{\lambda}$ is the average path length of the electrons in the presence of the excited target, ρ_{Mg^*} is the average density of Mg 3^1P, and σ_{SES} is the superelastic scattering cross section as described above. At threshold energies, the electron does not have time to leave the interaction region prior to the decay of the 3^1P target. Hence, the effective path length of the electrons through the target gas was determined by considering the velocity of REMPI electrons and the lifetime of the target atoms' excited state, with a correction of the electron velocity due to the space charge effect. The correction for the path length is calculated at energies below 170 meV using an average over the population of the 3^1P state and the lifetime of the laser. A Gaussian distribution with ΔE of 6 meV is used to calculate the effective path length, and the excitation profile for the 3^1P state is used to find the effective pulse length. This means that an electron with zero energy has an effective path length of 6.6×10^{-3} cm, although this correction had no significant effect on the determined energy dependence. The target density is determined from the strength of the REMPI signal.

3. Results

The first set of experiments were done with a single laser frequency, resonant with the excitation energy of the 3^1P state of Mg at 4.35 eV. A characteristic electron TOF spectrum for a one-color experiment is shown in Figure 3. In this experiment,

TABLE 1: One-Color, Resonant and Nonresonant Relative Laser Dependence for Peaks A, B, D, E, and F[a]

	one-color intensity dependence				
	I_1	I_2	I_3	I_4	I_5
intensity (W/cm^2)	670 ± 70	1100 ± 110	2200 ± 220	3400 ± 340	6800 ± 680
I^{R+1}	1.0	3.2 ± 0.3	6.8 ± 0.7	13.2 ± 1.3	30 ± 3.0
I^{2R+1}	1.0	**3.6 ± 0.4**	**14.8 ± 1.5**	**30.4 ± 3.0**	**80 ± 8.0**
REMPI	1.0	2.8 ± 0.3	6.4 ± 0.6	12.4 ± 1.2	29.2 ± 2.9
peak A	1.0	**4.0 ± 0.4**	**14.8 ± 1.5**	**28.8 ± 2.9**	**86 ± 8.6**
peak B	1.0	**4.2 ± 0.4**	**11.2 ± 1.1**	**35.6 ± 3.6**	**71.6 ± 7.2**
	two-color resonant intensity dependence				
	I_1	I_2	I_3	I_4	
intensity (W/cm^2)	600 ± 60	1060 ± 100	1680 ± 170	2360 ± 240	
$\Delta\rho_{Mg^*}$	1.0	1.5 ± 0.1	2.0 ± 0.2	2.3 ± 0.2	
$(\Delta\rho_{Mg^*})^2$	1.0	**2.4 ± 0.4**	**4.0 ± 0.4**	**5.2 ± 0.5**	
peak D_{res}	1.0	**2.3 ± 0.2**	**3.6 ± 0.2**	**4.7 ± 0.5**	
peak E_{res}	1.0	1.3 ± 0.1	1.8 ± 0.3	2.1 ± 0.2	
peak F_{res}	1.0	**2.6 ± 0.3**	**3.7 ± 0.3**	**4.6 ± 0.5**	
	two-color nonresonant intensity dependence				
	I_1	I_2	I_3		
intensity$_{nr}$ ($\times 10^6 W/cm^2$)	6.3 ± 0.6	10 ± 1	21 ± 2		
relative intensity$_{nr}$	1.0	1.6 ± 0.2	3.2 ± 0.3		
REMPI$_{nr}$	1.0	1.8 ± 0.2	3.5 ± 0.4		
peak D$_{nr}$	1.0	1.5 ± 0.2	3.6 ± 0.3		
peak E$_{nr}$	1.0	**2.7 ± 0.3**	**8.6 ± 0.8**		
peak F$_{nr}$	1.0	1.4 ± 0.2	3.4 ± 0.3		

[a] I^{R+1} is the expected dependence for a two-photon process with one resonant and one nonresonant transition; I^{2R+1} is that for a three-photon process with two-photon resonant and one photon nonresonant process. The change in excited-state density, $\Delta\rho_{Mg^*}$ is shown for reference for the resonant case. Boldface type indicates the result is consistent with the higher order process, either I^{2R+1} or a quadratic dependence on intensity; normal type indicates a linear dependence or I^{R+1}.

TABLE 2: One- and Two-Color Relative Density Dependence for Peaks A, B, D, E, F, and REMPI

	electron count rate with changing density		
process	low Mg density	intermediate Mg density	high Mg density
REMPI	1.0	2.3 ± 0.2	8.0 ± 0.8
peak A	1.0	**8.5 ± 0.8**	**50 ± 5**
peak B	1.0	**6.1 ± 0.6**	**48 ± 5**
peak D	1.0	**3.1 ± 0.4**	**49 ± 5**
peak E	1.0	2.3 ± 0.3	8.5 ± 0.8
peak F	1.0	**4.4 ± 0.3**	**50 ± 5**

[a] Count rates are measured at low, intermediate, and high temperatures resulting in a corresponding change in mg density. Boldface type indicates a quadratic dependence on density, normal type indicates a linear dependence on density.

REMPI electrons are produced with an energy of 1.04 eV, which corresponds to peak C in Figure 3. The TAC is saturated by the REMPI signal; therefore, peak C is truncated. The electrons in peak A have the energy of one additional resonant photon, 5.40 eV. The possible mechanisms which yield electrons of this energy are SES of two-photon REMPI electrons from the 3^1P state to the ground state or three-photon ATI. Peak B arises from a SES event in which the Mg de-excites from the 3^1P state to the 3^3P state, 2.70 eV. These peaks correspond to the de-excitation processes indicated in eqs 5 and 6, respectively.

The SES assignment in the one-color experiment is verified by the laser intensity dependence, shown in Table 1, and the Mg density dependence, shown in Table 2. The intensity dependence data from one-color experiments is consistent with a process which requires one ionization photon plus two resonant photons (SES) as opposed to two nonresonant photons plus one resonant (ATI). The 3^1P excited-state is produced by a resonant transition which, because of saturation, shows a dependence on laser intensity that deviates from linear at high laser power. The dependence can be predicted through the expression for the excited-state population in eq 9 [41]

$$\frac{N_2}{N} = \frac{\bar{W}}{\frac{\eta\omega^3}{\pi^2 c^3} + 2\bar{W}}\left\{1 - \exp\left(-\left(\frac{\eta\omega^3}{\pi^2 c^3} + 2\bar{W}\right)t\right)\right\} \qquad (9)$$

where $\bar{W} = \bar{I}/c\delta\omega$, $\delta\omega$ is the experimental bandwidth and is 7×10^{11} Hz, N_2/N is the relative excited-state population, ω is the transition frequency, $\bar{I}$ is the average photon intensity, c is the speed of light, η is the index of refraction, and t is the time.

The most straightforward evidence for the proper assignment of the observed mechanism as SES is the quadratic Mg density dependence shown in Table 2. The density range is relatively small because of limitations on ionization rates to minimize the space charge effect and ATI. The density dependence is expected to be linear for REMPI and ATI but quadratic for SES. Table 2 shows quadratic dependencies for peaks A and B (SES), which supports the interpretation that the dominant mechanism for both these peaks is two-photon REMPI followed by SES, with the free electron colliding with an excited Mg atom. The intensity of peak C (not shown) is linear in Mg density.

The cross section for the 270 meV electrons has been normalized to the values from the **R** matrix calculations of Sullivan et al.[9] The normalization factor, determined at 0.27 eV for the 3^1P to 3^1S channel, is used to determine the cross section of SES from the 3^1P state to the 3^3P and the cross sections for the energy dependence study of both transitions. The difference between the renormalized and the directly measured experimental values is a factor of 12, the greater for the unnormalized measured values. The difference is larger than expected, and the origin of the discrepancy is not clear, to say

TABLE 3: Measured Space Charge Effect as a Function of Electrons Per Pulse

electrons/pulse	space charge energy (meV)
2400	22
1074	13
518	5

the least; however, it is likely associated with the combined uncertainties of the ground state atomic density, the electron path length, and the collection efficiency of the MBS.

An uncertainty of about 40% is associated with the absolute determination of the 3^1P density. This error includes the uncertainty in the efficiency of the spectrometer ϵ, in the measured photoionization cross section σ_{Ion}, in the volume V of the interaction region, in the photon flux Φ, and in the pulse duration τ. The density is determined from the measured rate of REMPI electrons in eq 10.

$$R_{\mathrm{REMPI}} = \epsilon\sigma_{\mathrm{Ion}} V \rho_{\mathrm{Mg}^*} \Phi\tau \tag{10}$$

A second complication associated with the use of a MBS is the uncertainty in the path length of the electron in the presence of the excited target. Below 175 meV, the electron is slow enough that the excited Mg may de-excite before the electrons have left the interaction region. The effective path length is only a function of the lifetime of the excited-state and the velocity of the electron. For electrons with less than 175 meV of energy, the sum of the lifetimes of the laser pulse and the average lifetime of the excited-state is larger than the lifetime of the electron inside the interaction region. Therefore, the effective path length may be calculated using the electron energy, its uncertainty, and the lifetime and average population of the excited state. This also means that the pulse width of the laser is critical in determining the correct cross section. For electrons with more than 175 meV of energy, the magnetic field affects the trajectory and hence the effective path length. Electrons emitted along the axis of the MBS in the direction of the detector have the minimum path length inside the interaction region of 0.078 cm, while electrons ejected perpendicular to the MBS axis spend a period of time nearly equal to the duration of the excited state in the interaction region. The average path length in the interaction region for a 1.05 eV electron is 0.23 cm, a 2.9-fold increase from the minimum path length.

It is important to recognize here that the principal contributor to the linewidths of the arrival time distributions is the variations in path lengths which, in turn, are due to the different directions in which the electrons are emitted, causing differences in (the distributions and histories of) their longitudinal velocities. Hence, it is possible to use analysis of the arrival time line shapes to determine the angular distributions of the emitted electrons, so long as they do not suffer significant scattering as they leave the reaction chamber. This approach, coupled with the use of varied polarizations of the ionizing radiation, could be a useful tool in experiments of the kind described here. Simulated lineshapes indicate that such determinations would be practical with apparatus of the general kind employed in these experiments.

The determination of the incident electron energy resolution hinges on evaluating the effect of space charge in the interaction region.[2] The space charge effect causes broadening in the energy distribution of the incident electrons (photoelectrons) from Coulomb interactions between the electrons and the cations in the region.[40] The broadening of the resolution by ion space charge can be estimated by calculating the potential variation,

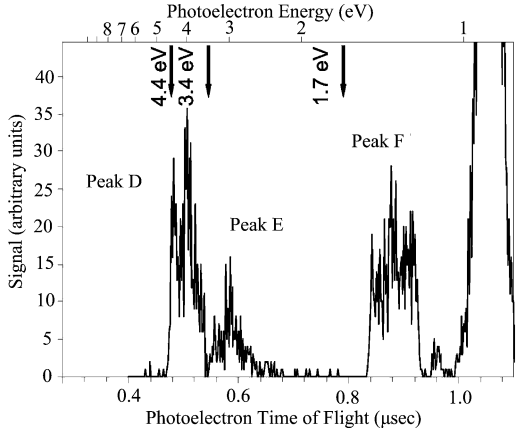

Figure 4. Two-color time-of-flight spectrum for 285.21 nm (2000 W/cm^2) and 370.45 nm light (6×10^6 W/cm^2) with a Mg density of 8×10^{10} atoms/cm^3. Peaks A and B of Figure 3 due to SES by the 3^1S and 3^3P states are essentially invisible here. Peaks D and F are due to electrons from two-color REMPI followed by SES to the 3^1S and 3^3P states, respectively. Peak E is caused by two-photon ATI from the 3^1P state.

ΔV, within a sphere of radius R and homogenously charged with Q elementary charges

$$\Delta V = 0.0009\frac{Q}{R} \tag{11}$$

where ΔV is in meV, R is 0.6 mm, and $Q = 950$ electrons resulting in a ΔV of 2 meV for the threshold electron experiment. This estimate does not take into account the suppression of the effect by the oppositely charged ions. Therefore, the broadening effect is expected to be lower than this estimate. Furthermore, previous work by Klar et al. has shown that photoelectron resolution for the photoionization of Ar results in sub-millielectron volts resolution, which supports our claim that space charge effects are small enough to be neglected.[42] The interaction region space charge effect is thus at the resolution limit of the spectrometer.

The incident electron energy resolution was estimated at 1 meV for the threshold experiments by producing electrons of different energies to investigate the broadening that occurs in the interaction region. Broadening that occurs after the electron exits the interaction region can also be observed in the TOF spectrum, but much of this broadening does not occur inside the interaction region. The results of the resolution study as a function of ions produced per pulse is shown in Table 3. Additional but less important factors contributing to the resolution include the Doppler motion of the scattering target and the bandwidth of the photoionization radiation.

A characteristic TOF spectrum for a two-color experiment is shown in Figure 4. Peaks A and B of Figure 3, which correspond to the one-color SES processes, are barely visible here, because the laser intensities were set so that the two-color processes dominate strongly. Peak D is the SES of the two-color photoelectrons from the 3^1P to the ground state involving the tunable ionizing laser. Peak E corresponds to the energy of the two-color, two-photon ATI from the 3^1P state, and peak F is SES from the 3^1P to the 3^3P state, also involving the tunable ionizing laser. Table 2 shows the density dependence of these processes in the two-color experiment; peaks D and F show a quadratic dependence on the density that confirms their initial characterization as SES processes. The third process shows a linear relation with density, thus, confirming the ATI assignment. The dependence on laser intensity is shown in Table 1.

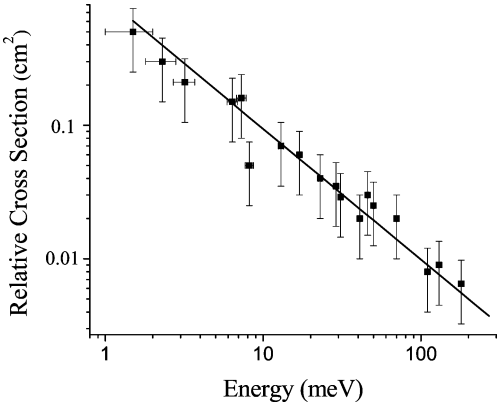

Figure 5. Cross sections for the energy dependence study for the transition to the 3^1S level. The fit plots the energy dependence as $7.5 \times 10^{-13}E^{-0.98}$. The absolute cross sections have been normalized to the R matrix calculations of Sullivan et al.[9] at 270 meV.

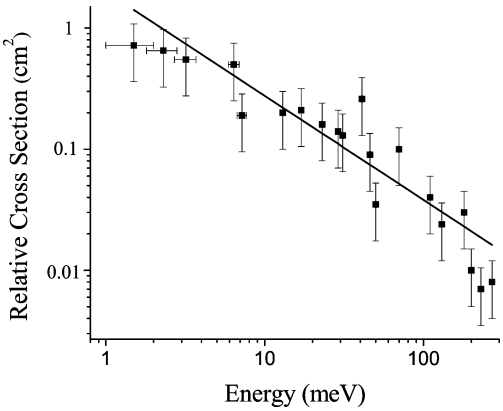

Figure 6. Cross sections for the energy dependence study for the transition to the 3^3P level. The fit plots the energy dependence as $1.4 \times 10^{-12}E^{-0.85}$.

Table 1 shows that peak E, the peak assigned as ATI, is linear in light intensity and that peaks D and F depend quadratically on the intensity of the resonant radiation. On the other hand, Table 1 shows the nonresonant laser intensity dependence and that the SES signals are linear with respect to the nonresonant radiation intensity and the ATI process has a quadratic dependence. These laser and atomic density dependence studies allow us to characterize peaks D and F as being due to SES and characterize peak E as the result of ATI.

Relative cross sections for the 3^1P to 3^1S transition are shown in Figure 5, while those for the transition to the 3^3P state are shown in Figure 6. The resolution of the incident electron is 1 meV at 1.5 meV and grows to 6 meV at 1.05 eV. The significant decrease in the cross section at higher energy required using higher laser intensities, causing the ionization rate to increase, which in turn increased the space charge effect. The error bars represent a 50% uncertainty in the apparent absolute cross sections. The energy dependence of the 3^1P to 3^1S transition is described by $\sigma_{SES} \propto E^{-1.0\pm0.1}$ cm^2 and that of the 3^1P to 3^3P transition is $\sigma_{SES} \propto E^{-0.9\pm0.1}$ cm^2. The normalization factor for the raw data would be 1.1×10^{-12} for the 3^1S channel and 3.0×10^{-12} for the 3^3P channel, and if normalized to the work of Sullivan et al., the normalization would be 8.9×10^{-14} for the 3^1S channel and 2.5×10^{-13} for the 3^3P, although uncertainties in the absolute measurements prevent using this as a valid total cross section.

The near-threshold region of the energy dependence is expanded in Figure 7 to show the change in energy dependence for the transition to the 3^3P and 3^1S state. Figure 7 has been

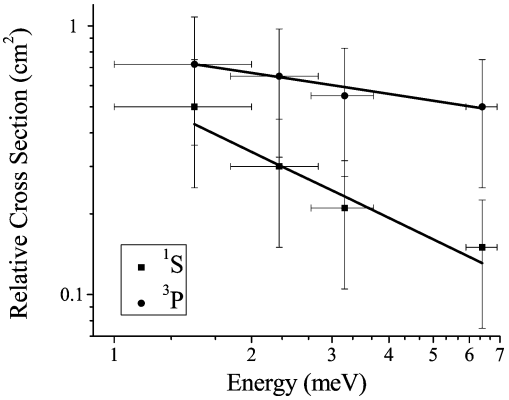

Figure 7. Cross sections for the threshold region for transition to both 3^1S and 3^3P levels. The fit for the 3^1S channel is $5.3 \times 10^{-13}E^{-0.81}$, and the fit for the 3^3P channel is $6.6 \times 10^{-12}E^{-0.3}$.

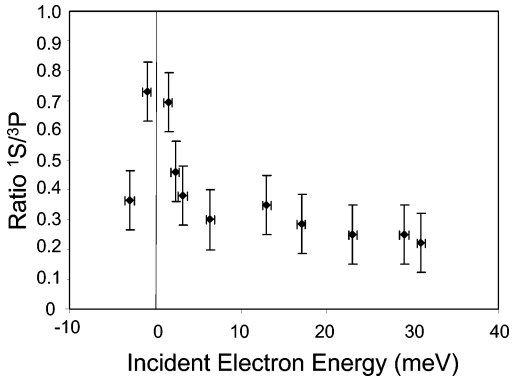

Figure 8. Ratio of the 3^1S to 3^3P rates in the threshold region.

made by combining the data from two experiments, the cross section results shown in Figures 5−7 and a second experiment in a single run with sub-threshold measurements where the data from the single run has been normalized to the cross section data. The energy dependence of the transition from the 3^1P to 3^3P is different from that of the transition to the ground state, which is measured simultaneously. The determination of the absolute energy and resolution of the electron energy are critical for analysis near the threshold. Figure 8 shows the branching ratio for electron signal associated with SES. At the threshold energy for ionization from the 3^1P state, a sharp peak, a sort of resonance, almost a discontinuity in the branching ratio, occurs. Above threshold, where the two decay processes are equivalent, the ratio gradually passes to a condition in which decay to the 3^3P state dominates.

4. Discussion

A change in the energy dependence of the SES cross section at less than 10 meV occurs in only one channel. The simultaneous measurements allow greater confidence to address this feature, and we conclude that there is a difference in the energy dependence between these two decay channels at energies below 10 meV above threshold. At threshold, two significant features of this experiment change. The first is that the photoabsorption spectra for continuum states is significantly higher than for Rydberg states.[43] Second, this lower cross section causes a build up in the excited 3^1P state. This is seen in the increase in the ionization rate for multiphoton ionization rate versus ATI due to this increased population of 3^1P state.[35] This causes a compression in the energy of the available electrons toward threshold. Also, the difference in mechanism in which the 3^3P channel is dominated by an exchange process, and the direct

TABLE 4: Comparison of Mg Superelastic Scattering Cross Section for ^1P to ^1S State Where the Inelastic Cross Sections of Leep and Gallagher[10] and Sullivan et al.[9] Have Been Converted to Superelastic Scattering Cross Sections Using Eq 12

energy	De Broglie	ref 10	ref 9 (calcd)	ref 9	present work
1.05 eV	1.1×10^{-13}	6.6×10^{-16}	1.6×10^{-15}	1.7×10^{-15}	3.1×10^{-15}
270 meV	1.7×10^{-12}		1.5×10^{-15}	1.8×10^{-15}	3.3×10^{-14}
150 meV	5.5×10^{-12}		1.8×10^{-15}	1.4×10^{-15}	6.0×10^{-14}

collision to the ground state is almost certain to play some role in this result. For example, if we think of the Rydberg 3^1P process as involving a virtual photon, the dipole coupling between these two states are much weaker than between continuum, while 3^1P-3^3P transition is an exchange process.

A striking feature of this result is that the energy dependence for production of the triplet appears to be different from that of the expected $E^{-1/2}$ dependence for the basis of an S wave collision in the 3^1S channel. The result means that extra caution must be taken to be certain that the threshold dependence is what has been measured. The **R** matrix calculations of Sullivan et al. for the time-reversed process show $E^{1/2}$ dependence,[9] which implies the expected $E^{-1/2}$ dependence in the SES process. This is not unexpected for an **R** matrix calculation, where the inner and outer regions are separated in the same way as in the determination of the threshold law. The experimental results of Sullivan et al. seem to show a dependence on energy higher than the $E^{1/2}$ expected for the inelastic process.

The determination of the electron energy resolution is critical to determining the path length and hence the cross sections near threshold. By using the branching ratio between the 3^1S and the 3^3P channels, it appears that the energy resolution at low energies is better than 1 meV. The branching ratio as a function of energy is shown in Figure 8 and is found to be nearly constant from 10 to 270 meV, with a slight increase between 10 meV and threshold. This ratio changes by a factor of 2 at threshold. The energy dependence in the feature changes sharply at 0.5 meV, thus, demonstrating that the resolution is 1 meV at threshold. The energy resolution must be close to the estimated resolution, 1 meV, to observe the change in the energy dependence from threshold to 10 meV.

There are several possible explanations for the unexpected dependence. One possibility that we believe unlikely is that the true velocity of the electrons within the interaction region could conceivably be higher than expected, specifically for the very slow electrons. Because the excited atom de-excites before the electron leaves the interaction region and could energize the projectile electron in the process, such an increase in the electron energy would result in a longer path length in the interaction region and a larger number of collisions between electrons and excited Mg. Consequently, the determined cross section would be too high, certainly higher than that of the truly slow electrons. Furthermore, for this to be the source of the energy dependence, the excess electron energy must change as a function of photon energy, rather than just adding a constant uncertainty.

A second possibility, which we also consider unlikely, could be a consequence of the electromagnetic field of the resonant laser source. While we believe the laser intensity in these experiments is too low for the three-body laser-assisted collision to be significant, the work of Purohit and Mathur shows that significant intensities (10^{11} W/cm^2) of resonant light may increase the measured cross section up to 4 orders of magnitude.[44] If the field were to have an effect on the slow electrons, this might also help explain the large normalization factor. It is possible that this process has a higher probability with slower electrons in the immediate vicinity of atoms, and that it could affect the energy dependence of the SES cross sections.

The factor we think is most likely to give rise to the change in energy dependence of the channel producing atoms in the 3^3P state lies in the difference in the processes yielding the two final channels. It should be noted that the 3^3P channel is likely caused by an exchange process, while the 3^1S channel is most likely from a direct scattering process. Furthermore, this effect occurs as the channel for Rydberg state scattering opens. This difference in mechanism is what we think is most likely to account for the difference in the two channels.

An additional reason for the difference may simply be the range over which the threshold law is observed. In some experiments, the threshold law only manifests itself well below 1 meV,[24] so we may be measuring a dependence, but we have not yet reached the energy region which demonstrates the threshold law.

On the basis of the thorough characterization analysis of the observed processes of superelastic scattering and above-threshold ionization, we compare the superelastic cross sections to literature values for inelastic scattering (the time reverse process of superelastic scattering). Available literature values are limited to the works of Leep and Gallagher[10] and Sullivan et al.[9] based on energy range and resolution. The experimental literature results are based on traditional crossed beam techniques. Leep and Gallagher use a relative method and normalize to the Born approximation at high energy. The work of Sullivan et al. has used crossed-beam measurements and electron transmission spectroscopy, with results normalized to an **R** matrix calculation. Table 4 is a comparison among these results at 1.05 eV and 270 and 150 meV. The inelastic cross-sections are converted through time reversal to superelastic scattering cross-sections using eq 12

$$\left(\frac{\mathrm{d}\,\sigma}{\mathrm{d}\,\Omega}\right)_{\mathrm{for}} (2S_\mathrm{A}+1)(2S_\mathrm{B}+1)k_\mathrm{i}^2 = \left(\frac{\mathrm{d}\,\sigma}{\mathrm{d}\,\Omega}\right)_{\mathrm{rev}} (2S_\mathrm{C}+1)(2S_\mathrm{D}+1)k_\mathrm{f}^2 \quad (12)$$

where S_x indicates the spin of the reactants (A and B) and the products (C, D), and k_i and k_f are the densities of states in the initial and final channels. There is clearly a significant discrepancy between the absolute magnitudes of the results. The energy resolution of these studies might limit the type of feature and appropriate range of energy-dependent investigation but does not explain the difference in cross sections at these selected energies.

The technique used in this work has a limited uncertainty in the energy dependence and absolute cross-section in the threshold region. The parameters and efficiencies used to determine the cross section have a limited physically acceptable range, and the reported cross-section is close to the minimum cross-section capable within these physical limitations.

The largest uncertainties basic to this technique are the average electron path length through the excited medium, the number of incident electrons, and the density of atoms in the excited state. As threshold is approached, the energy of the electron defines the path length due to the short excited-state lifetime and laser pulse duration controlling the presence of the

excited-state density. The number of incident electrons and the density of the excited species are related. If the density of incident electrons were significantly higher than in these experiments, we would see a measureable broadening due to space charge effects (see eq 11). A direct measurement of rates R_j through time-of-flight spectroscopy significantly improves the capability to determine the number of unscattered electrons (R_0-R_s) similar to the technique of photon counting used by Sullivan (see eq 8). Normalization to either of these cross-sections at this time would be inappropriate, and the discrepancy seems irreconcilable without a drastic explanation, which needs to be consistent with the mechanism characterization. The explanation of photon induced or aided electron scattering processes, which has been shown to enhance the cross section by up to 4 orders of magnitude,[44] fails to be consistent with the characterization results. The photon enhancement (three-body collision) of the cross-section would be evident in the laser intensity dependence mechanism study. The resonant photon intensity used in this work is 2 orders of magnitude below the intensity used in the studies of Purohit and Mathur.

5. Conclusions

This method uses very slow photoelectrons with very narrow energy distributions, which opens a way to measure the threshold energy dependence of superelastic scattering, SES, and presumably other very low-energy scattering processes as well. The resolution of the low electron energy is achieved by using photoelectrons produced just above the ionization threshold. These then scatter on excited magnesium atoms in the focus of a magnetic bottle spectrometer. Combining a resonant-frequency excitation laser with a tunable laser to produce the photoelectrons, the cross sections of the available de-excitation channels may be measured as functions of energy, at high-energy resolution. An unexpected result was finding that the energy dependences of the 3^1S and 3^3P channels diverge at energies below 10 meV. The 3^1S channel follows a E^{-1} dependence at all measured energies, and the 3^3P channel has that same dependence above 10 meV, but varies as $E^{-1/2}$ below 10 meV.

The most notable result in the energy region of less than 10 meV is that observed difference in the energy dependence between the 3^3P and the 3^1S channels. The $l = 0$ angular momentum channel for the incoming electron is expected to dominate in both channels, and both channels should experience the same long-range potentials and consequently the same energy dependence. Electron correlation makes a significant contribution to the electron−atom interaction in this energy range.[35] The difference in behavior of the two channels may be a consequence of the requirement, for the triplet channel, either of a spin flip required for a direct collision process or of a low-energy phenomenon in electron exchange that is required for a transition to the 3^3P state. At threshold, it is also possible that effects of electron correlation could account for the change in the energy dependences and branching ratio as a function of energy between the 3^3P and the 3^1S levels with the latter channel demonstrating a dependence that is consistent with that of a dipole potential where the lowest eigenvalue is below the critical value.[30] The most striking result is that the energy dependencies in the two channels are different in this energy region.

Acknowledgment. This work was supported by the National Science Foundation, two GAANN fellowships (A.R. and S.D.), and two National Science Foundation Fellowships (T.B. and S.D.). R.S.B. wishes to acknowledge the hospitality of the Aspen Center for Physics, where some of the preparation of the manuscript was done.

References and Notes

(1) Darveau, S.; Berry, R. S. *Resonance Ionization Spectroscopy*; American Institute of Physics: New York, 1998, p 253.
(2) Gallagher, A. C.; York, G. *Rev. Sci. Instrum.* **1974**, *45*, 662.
(3) Hertel, I. V.; Stoll, W. J. *J. Phys. B* **1974**, *7*, 570.
(4) Hertel, I. V.; Stoll, W. *J. Phys. B* **1974**, *7* 583.
(5) McClelland, J. J.; Kelley, M. H.; Celotta, R. J. *Phys. Rev. A* **1989**, *40*, 2321.
(6) Andersen, N.; Gallagher, J. W.; Hertel, I. V. *Phys. Rep.* **1988**, *16*, 1.
(7) Kruit, P.; Read, F. H. *J. Phys. E: Sci. Instrum.* **1983**, *16*, 313.
(8) Trajmar, S.; Nickel, J. C. *Adv. Atom. Mol. Opt. Phys.* **1993**, *30*, 45.
(9) Sullivan, J. P.; Burrow, P. D.; Newman, D. S.; Bartschat, K.; Michejda, J. A.; Panajotovic, R.; Moghbelalhossein, M.; McEachran, R. P.; Buckman, S. J. *New. J. Phys.* **2003**, *5*, 159.1.
(10) Leep, D.; Gallagher, A. *Phys. Rev. A* **1976**, *13* 148.
(11) Aleksakhin, I. S.; Zapesochnyi, I. P. *Opt. Spectr.* **1973**, *34* 611.
(12) Shpenik, O. B.; Zapesochnyi, I. P. *Sov. Phys. JETP* **1979**, *49* 426.
(13) Lin, C. C.; Anderson, L. W. *Adv. At. Mol. Opt. Phys.* **1991**, *32* 1.
(14) Li, Y.; Zetner, P. W. *J. Phys. B* **1995**, *28* 5151.
(15) Gedeon, V.; Lengyel, V.; Zatsarinny, O.; Kocher, C. A. *Phys. Rev. A* **1999**, *59* 2016.
(16) Chutjian, A.; Alajajian, S. H. *Phys. Rev. A* **1985**, *31* 2885.
(17) Bommels, J.; Leber, E.; Gopalan, A.; Weber, J. M.; Barsotti, S.; Ruf, M.-W.; Hotop, H. *Rev. Sci. Instrum.* **2001**, *72*, 4098.
(18) Hoffmann, S. V.; Lunt, S. L.; Jones, N. C.; Field, D.; Ziesel, J.-P. *Rev. Sci. Instrum.* **2002**, *73*, 4157.
(19) Field, D.; Knight, D. W.; Mrotzek, G.; Randell, J.; Lunt, S. L.; Ozenne, J. B.; Ziesel, J.-P. *Meas. Sci. Technol.* **1991**, *2*, 757.
(20) Jacka, M.; Kelly, J.; Lohmann, B.; Buckman, S. J. *J. Phys. B* 1995, *28*, L361.
(21) Jacka, M.; Hoogerland, M. D.; Lu, W.; Milic, D.; Baldwin, K. G. H.; Bartschat, K.; Buckman, S. J. *J. Phys. B* **1997**, *29*, L825.
(22) Berry, R. S.; Reimann, C. W. *J. Chem. Phys.* **1963**, *38*, 1540.
(23) Lineberger, W. C.; Woodward, B. W. *Phys. Rev. Lett.* **1970**, *25*, 424.
(24) Slater, J.; Read, F. H.; Novick, S. E.; Lineberger, W. C. *PRA* **1978**, *17*, 201.
(25) Dunning, F. B. *J. Phys. Chem.* **1987**, *91*, 2244.
(26) Kozhekin, A.; Kurizki, G.; Sherman, B *Phys. Rev. A* **1996**, *54*, 5435.
(27) Wigner, E. P. *Phys. Rev.* **1948**, *73*, 1002.
(28) Landau, L. D.; Lifshitz, E. M. *Quantum Mechanics (Non-relativistic Theory);* Butterworth-Heinemann: Oxford, 1998.
(29) Gailitis, M.; Damburg, R. *Proc. Phys. Soc.* **1964**, *82*, 192.
(30) Sadeghpour, H. R.; Bohn, J. L.; Cavagnero, M. J.; Esry, B. D.; Fabrikant, I. I.; Macek, J. H.; Rau, A. R. P. *J. Phys. B* **2000**, *33*, R93.
(31) Rau, A. R. P. *Comments At. Mol. Phys.* **1984**, *14*, 285.
(32) Agostini, P.; Fabre, F.; Mainfray, G.; Petite, G.; Rahman, N. K. *Phys. Rev. Lett.* **1979**, *42*, 1127.
(33) Reber, A.; Martín, F.; Bachau, H.; Berry, R. S. *Phys. Rev. A* **2003**, *68*, 063401.
(34) Reber, A.; Baynard, T.; Martín, F.; Bachau, H.; Berry, R. S. *Phys. Rev. A* **2005**, *71*, 053402.
(35) Reber, A.; Gordon, C.; Berry, R. S. *Phys. Chem. Chem. Phys.* **2005**, *7*, 3226.
(36) Madsen, D. N.; Thomsen, J. W. *J. Phys. B* **2002**, *35*, 2173.
(37) Cheshnovsky, O.; Yang, S. H.; Pettiette, C. L.; Craycraft, M. J.; Smalley, R. E. *Rev. Sci. Instrum.* **1987**, *58*, 2131.
(38) Tsuboi, T.; Xu, E. Y.; Bae, Y. K.; Gillen, K. T. *Rev. Sci. Instrum.* **1988**, *59*, 1357.
(39) Moccia, R.; Spizzo, P. *J. Phys. B* **1988**, *21*, 1131.
(40) Zimmerman, B. *Record of 10th Symposium on Electron Ion and Laser Beam Technology*; San Francisco Publishing Company: San Francisco, CA, 1969.
(41) Loudon, R. *The Quantum Theory of Light;* Oxford University Press: New York, 2000.
(42) Klar, D.; Ruf, M.-W.; Hotop, H. *Meas. Sci. Technol.* **1994**, *5*, 1248.
(43) Yih, T.-S.; Wu, H.-H.; Chan, H.-T.; Chu, C.-C.; Pong, B.-J. *Chin. J. Phys.* **1989**, *27*, 136.
(44) Purohit, S. P.; Mathur, K. C. *Phys. Rev. A* **1992**, *45*, 6502.